ACS Photonics

Article

pubs.acs.org/journal/apchd5

Plasmon-Enhanced Emission Rate of Silicon Nanocrystals in Gold Nanorod Composites

Hiroshi Sugimoto,[†,‡] Tianhong Chen,[§] Ren Wang,[†] Minoru Fujii,[‡] Björn M. Reinhard,[§] and Luca Dal Negro*[,†,∥]

[†]Department of Electrical and Computer Engineering & Photonics Center, Boston University, 8 Saint Mary Street, Boston, Massachusetts 02215, United States

[‡]Department of Electrical and Electronic Engineering, Graduate School of Engineering, Kobe University, Rokkodai, Nada, Kobe 657-8501, Japan

[§]Department of Chemistry & Photonics Center, Boston University, Boston, Massachusetts 02215, United States

[∥]Division of Materials Science and Engineering, Boston University, 15 Saint Mary's Street, Brookline, Massachusetts 02446, United States

Supporting Information

ABSTRACT: We develop colloidal nanocomposites consisting of coupled light-emitting Si nanocrystals (NCs) and Au nanorods and systematically investigate their structural and photoluminescence (PL) properties, which demonstrate significant enhancement of spontaneous emission rate with suppressed nonradiative quenching. In addition, through a comparison of the polarization dependence of PL and scattering intensities of single nanocomposites, we successfully demonstrate that the emission from Si NCs coupled to Au nanorods is highly polarized along the major axis of nanorods. The experimental results in combination with rigorous simulations of dipolar emission in the vicinity of Au nanorods enable us to demonstrate a ~3 times enhancement of the quantum efficiency at the peak of the NC emission. The Si-based active plasmonic-coupled nanocomposites developed in this work provide novel opportunities for biocompatible platforms that leverage nanoscale fluorescent probes for biosensing and bioimaging device applications.

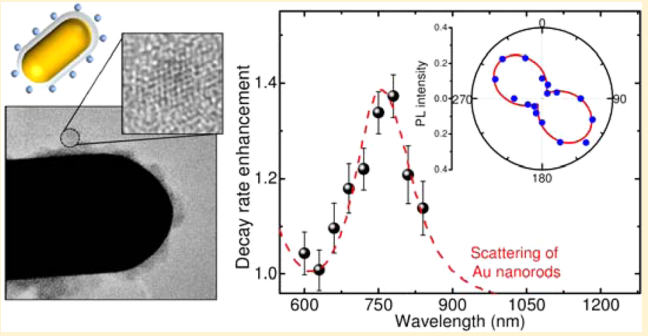

KEYWORDS: *silicon nanocrystals, plasmon, nanorod, colloid*

Plasmonic nanostructures including nanospheres, nanorods, nanodisks, and their arrays have been tailored to control the emission properties of organic dyes and semiconductor nanocrystals (NCs).[1,2] Significant light emission enhancement has been previously demonstrated utilizing the enhanced local field originating from localized surface plasmon resonance (LSPR) of metal nanostructures. The combination of plasmonic nanoparticles and nanoscale emitters into a single multifunctional colloidal platform has a large potential for the engineering of novel active devices for biosensing and bioimaging.[3−5] For such applications, semiconductor NCs possess superior properties compared to organic dyes in terms of size-tunable luminescence, resistance to degradation in aqueous solutions, and photostability.[6,7] Plasmon-enhanced emission of NCs with a Au nanoshell,[3] DNA-linked Au nanoparticles−NCs hybrid structures,[8] and Au nanorods coupled to NCs[9,10] in aqueous solutions have been demonstrated. However, the toxicity of these NC systems raises concerns for applications in biology and consumer optoelectronic devices and then demands focused efforts aimed at developing alternative solutions.[11,12]

Silicon (Si) NCs are the most promising alternatives to toxic II−VI and IV−VI semiconductors because of their compatibility with biological substances and the well-established Si technology. Plasmonic-coupled emission of Si NCs embedded in solid matrices has been widely investigated in the past decade.[13−17] In contrast, colloidal Si NCs coupled to plasmons have been scarcely studied in spite of their importance in applications such as in vivo bioimaging[18] and printable optoelectronics.[19,20] The development of such systems is still challenging due to the difficulty of synthesis of high-quality Si NCs with bright emission in biological transparent windows (700−1200 nm) and colloidal stability in aqueous solutions.[21,22]

Recently, we have developed a new type of colloidal Si NCs by inorganic surface functionalization with boron (B) and phosphorus (P).[23] We have demonstrated their size-tunable photoluminescence (PL) in a very wide wavelength range (600−1400 nm)[24] originating from donor−acceptor transitions

Received: April 30, 2015
Published: August 4, 2015

DOI: 10.1021/acsphotonics.5b00233
ACS Photonics 2015, 2, 1298−1305

due to B and P co-doping[25,26] and PL lifetimes of 10−200 μs, which are in the range of lifetimes commonly observed in Si NCs.[27−29] Co-doped Si NCs are well dispersed in water and exhibit excellent pH- and photostability of PL.[30]

In this work, we combine Si NCs and colloidal plasmonic particles to achieve enhanced and highly polarized light emission in an aqueous solution. In particular, we focus on the radiative rate engineering of Si NCs coupled to Au nanorods. It is well known that the enhanced local electric field in the vicinity of plasmon nanoantennas results in an increase of the local density of photonic states (LDOS),[31,32] which leads to the enhancement of the radiative decay rate of antenna-coupled emitters. This coupling effect boosts the quantum efficiency by overcoming the fast relaxation into nonradiative decay channels.[31,32] In this work, we present a facile synthesis of composites of colloidal Au nanorods decorated with Si NCs by electrostatic interaction. Detailed PL studies including decay time at different emission wavelengths show enhancement of the spontaneous emission rate in the absence of nonradiative quenching by properly tuning the separation between NCs and metallic nanorods. Furthermore, the emission from individual NC−nanorod composites exhibits the same polarization dependence as the light scattering of the longitudinal plasmon mode of Au nanorods. These results, in combination with theoretical calculations of radiative and nonradiative rates based on the boundary element method,[33] enabled us to accurately quantify the emission enhancement of the radiative rate of Si NCs coupled to Au nanorods. This work demonstrates that Si-based plasmonic-coupled nanocomposites are a very promising platform for biocompatible active device applications to sensing and spectroscopy.

SAMPLE PREPARATION

Colloidal Si NCs of two different sizes were prepared by the method described in detail elsewhere.[23,30] Si-rich borophosphosilicate glass (BPSG) was deposited by cosputtering Si, SiO_2, B_2O_3, and P_2O_5 in an rf-sputtering apparatus. The films were peeled off from the plates and annealed at different temperatures (1075 and 1150 °C) in a N_2 gas atmosphere for 30 min to grow Si NCs in BPSG matrices. The NCs were isolated from the matrices by dissolving in HF solution (46 wt %). Isolated Si NCs were then transferred and redispersed in water. The average diameters of Si NCs grown at 1075 and 1150 °C were 3.3 ± 0.9 and 4.6 ± 1.3 nm, respectively (see Figure 1). The NCs are well-dispersed in water without organic ligands. Our previous works[34,35] revealed that heavily co-doping with B and P is responsible for the colloidal stability and bright near-IR emission. Positively charged polymer-coated Au nanorods (A12-40-750-POS) were purchased from Nanopartz Inc. (Loveland, CO, USA) and used as received. A representative transmission electron microscope (TEM) image is shown in Figure 1c. The average length and width of the nanorods were 131 ± 8 and 57 ± 5 nm, respectively. Note that the size of nanocomposites developed in this work is in the acceptable range for bioimaging applications.[36] A uniform polymer layer can be seen in the inset. The average thickness of the polymer layer is 8 nm, with a standard deviation of 30%, which plays a crucial role in plasmonic coupling between NCs and nanorods.

Colloidal Si NCs prepared in this work are negatively charged (−25 mV in water at pH 7)[30] and Au nanorods are positively charged (+35 mV in water at pH 7). Therefore, by mixing 25 μL of Si NC solution (1 × 10^{16} NCs/mL) with 1.5 mL of concentrated Au nanorod solution (1.7 × 10^{10} nanorods/mL) for 2 days, NCs attach to the surface of the nanorods by electrostatic interaction.[37] The mixed colloidal solution was subjected to centrifugation to remove unattached NCs, and NC-decorated Au nanorods were redispersed in DI water.

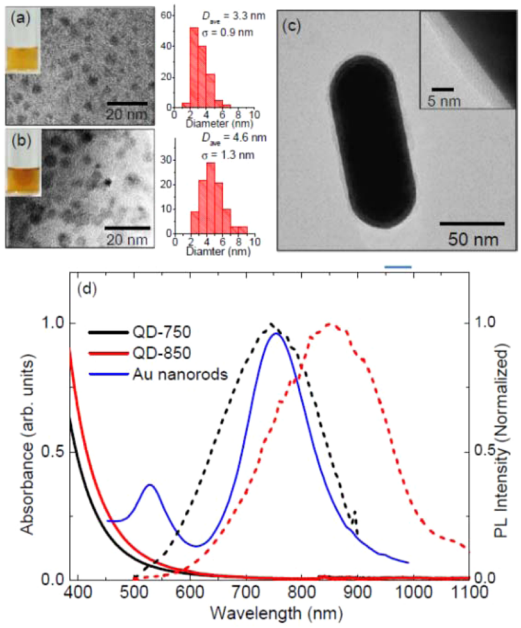

Figure 1. (a, b) Photographs and TEM images of Si NCs of different size. (c) TEM image of a positively charged polymer-coated Au nanorod. The inset shows a nanorod coated by a polymer layer. (d) Absorbance (solid) and normalized PL spectra (dashed) of Si NCs-750 (black) and Si NCs-850 (red) and the extinction spectrum of Au nanorods (blue).

CHARACTERIZATION AND MEASUREMENTS

TEM observations (Tecnai Osiris, FEI) were performed for carbon-coated TEM meshes on which the solution containing Si NC-decorated Au nanorods was drop-cast. Absorption spectra of NCs and nanorods were acquired with a spectrophotometer (Cary 5000, Varian). Dark-field scattering and PL images of composites were obtained using an inverted microscope (IX71, Olympus) equipped with a high-resolution electron-multiplying charge-coupled device (EMCCD) (iXon^{EM}, Andor). For dark-field measurements, the samples were illuminated through an air dark-field condenser. To obtain PL images, a 100 W mercury lamp (U-LH100HG, Olympus) with a 10 nm bandpass filter centered at 430 nm was used as an excitation source. The excitation light was filtered using a proper long-pass filter, and only emission from composites was detected by the CCD. In this condition, Au nanorods without Si NCs do not show any PL in the images. Polarization dependence of scattering and PL images were taken with a polarization analyzer placed in front of the detector. The linear profile of each bright spot on the images was analyzed, and the peak values were used for intensity comparison (see Figure S2 in the Supporting Information). Photoluminescence spectra and decay dynamics were measured using a monochromator (Oriel Cornerstone 260, Newport) and photomultiplier tubes for visible (Oriel 77348, Newport) and near-IR (R5509-73, Hamamatsu) regions. The excitation source was electrically modulated light from a laser diode of 405 nm (IQ1A-100,

DOI: 10.1021/acsphotonics.5b00233
ACS Photonics 2015, 2, 1298−1305

Power Technology Inc.). All the measurements were carried out at room temperature.

RESULTS AND DISCUSSION

Figure 1d summarizes the optical properties of Si NCs and Au nanorods in water. The NCs with 3.3 and 4.6 nm diameters exhibit broad spectra peaked at 750 and 850 nm, respectively. In the following, we refer to the NCs emitting at two different wavelengths as NCs-750 and NCs-850. We find that the longitudinal LSPR of Au nanorods at 750 nm overlaps with the PL spectra in particular of NCs-750. The weak transverse mode is also observed at 525 nm.

In Figure 2a, we show the extinction spectra of Au nanorods in water before and after decoration with Si NCs. The longitudinal mode exhibits a slight red-shift of 6 nm. This is consistent with previous results[37] and attributed to the modification of the local refractive index induced by the attachment of the NCs. Figure 2b shows a representative TEM image of a single Au nanorod decorated with Si NCs that are attached on the surface of the nanorod by electrostatic attraction in solution. In both high-resolution TEM images in Figure 2c and d, the lattice fringes corresponding to {111} planes of the Si crystal can be clearly observed. These images demonstrate that single-crystalline Si NCs are attached to the Au nanorods. The average separation between NCs and nanorods estimated by inspecting several TEM images (shown in Figure S1 in the Supporting Information) is 8.7 nm. Figure 2e,f show the dark-field scattering and PL images collected from the same region of NCs-850 coupled to Au nanorods. The bright spots in the images correspond to the spatial locations of the composites. Since the scattering and PL signals originate from the same locations, they demonstrate the formation of active (light-emitting) nanocomposites driven by the scattering of the nanorods. However, a few spots in the scattering cannot easily be colocated in the PL images, due to the small PL signal that is originated by a reduced number of NCs at such particular locations.

Figure 3a and b display normalized PL spectra of Au nanorods decorated with Si-NCs-750 and Si-NCs-850. We also plot the PL spectra of reference (Si NCs without nanorods in water) and extinction spectra of Au nanorods. To investigate the spontaneous emission rate of NCs coupled to Au nanorods, we measured the PL decay curves in a wide wavelength range. Representative decay curves measured at 750 nm are shown in the inset of Figure 3a and b. We observe that even for the NCs that are not coupled with nanorods, the PL decay curves are not single-exponential functions because of the inhomogeneity introduced by surface defects and impurity doping.[24] In this

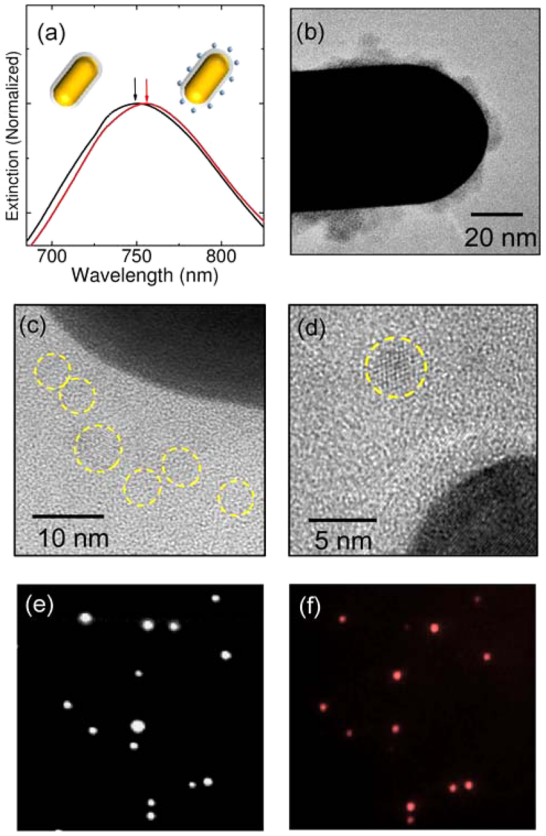

Figure 2. (a) Longitudinal LSPR peak of nanorods before and after decoration with Si NCs. (b) TEM image of Au nanorods decorated with Si NCs-850. (c, d) High-resolution TEM images of composites showing single-crystalline Si NCs attached to a nanorod surface with separation by a polymer spacer. (e) Dark-field scattering and (f) PL images of nanocomposites of Au nanorods and Si NCs-850 taken at the same region.

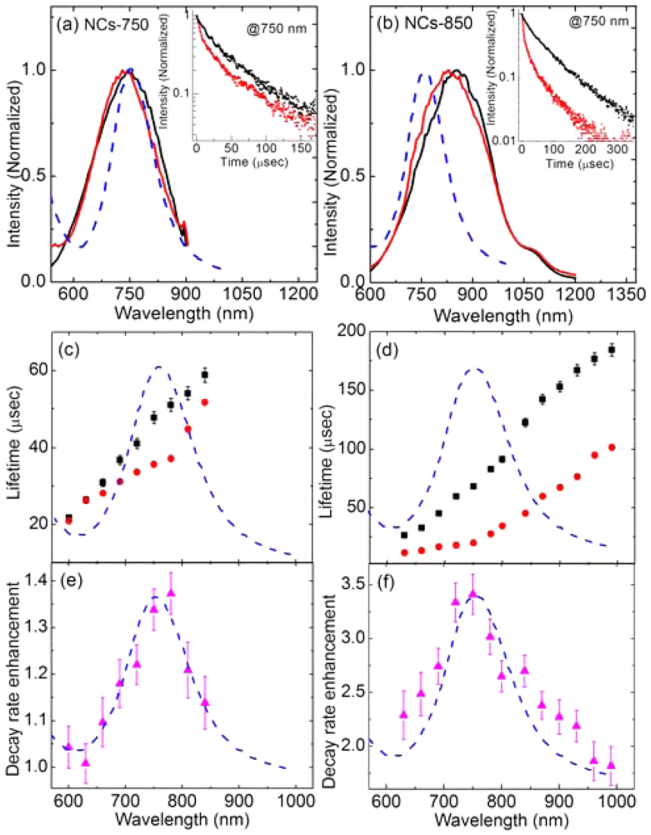

Figure 3. Normalized PL spectra of (a) NCs-750 and (b) NCs-850 coupled with Au nanorods (red line). Black and blue lines represent reference PL spectra of NCs in water and extinction spectra of Au nanorods, respectively. Inset: Representative decay curves detected at 750 nm. (c, d) Average PL lifetimes and (e, f) decay rate enhancement of NCs-750 (c, e) and NCs-850 (d, f) as a function of emission wavelength. Black squares and red circles in (c) and (d) are results for reference and NC-decorated Au nanorods. The error bars include the error during the fitting process.

DOI: 10.1021/acsphotonics.5b00233
ACS Photonics 2015, 2, 1298−1305

work, a stretched exponential function, $I = I_0 \exp[-(t/\tau)]^{\beta}$, where τ is the measurable decay constant and β is the stretching parameter of the decay, is used to estimate the lifetime of Si NCs with and without Au nanorods, which can be expressed by the Laplace transform of the decay rate distribution. The fitted β values varied from 0.55 to 0.85 for NCs coupled to nanorods, indicating a significant distribution of decay rates for each emission wavelength. According to the stretched exponential theory, an average lifetime can be defined as $\tau_{av} = \tau\beta^{-1}\,\Gamma(\beta^{-1})$, where Γ is the Euler gamma function.[38] In Figure 3c and e, we plot the average lifetimes of NCs with and without Au nanorods as a function of the detection wavelength. The lifetime of Si NCs increases monotonically with increasing the detection wavelength, as reported in the literature.[28,29,39] When the NCs are coupled to Au nanorods, the trend of lifetime is different from that of Si NCs alone. The lifetime is shorter only in the range 700−800 nm compared to the reference. The overall decrease of lifetimes of NCs-850 is observed in Figure 3d. To remove the intrinsic dependence of the NC lifetimes on wavelength, we approximate the decay rate with $\Gamma_{av} = \tau_{av}^{-1}$ and calculate the enhancement factors by considering the ratio of decay rates of NCs with and without Au nanorods. The decay rate enhancement values are shown in Figure 3e and f, which show a clear dependence on the emission wavelength due to the coupling with nanorods for both samples. The maximum enhancement reaches approximately 1.4 for NCs-750 and 3.4 for NCs-850. We notice that the measured enhancement values are larger where the PL spectra overlap with the longitudinal mode scattering spectrum of the LSPR of the nanorods. In Figure 3e, at an emission wavelength on either side of the peak, the decay rate enhancement factor approaches unity. This indicates that, irrespective of wavelength, the nonradiative energy transfer commonly observed for emitters positioned very close to metal (2−5 nm) surfaces[40,41] is suppressed by the presence of the polymer spacer layer. We performed the same measurements for NCs-750-decorated Au nanorods using a thinner polymer layer (see Figure S3 in the Supporting Information). In this case, the decay rate enhancement is approximately 3.5 for the overall PL spectrum. This proves that nonradiative decay channels are dominant for this sample. The decay rate enhancement of NCs-850 in Figure 3f also follows the extinction spectrum of the Au nanorods, but it is still greater than 1 (i.e., 1.8) even at wavelengths detuned from the resonance of Au nanorods. One possible explanation for this behavior is the agglomeration of NCs around the surface of nanorods, resulting in increased nonradiative recombinations.

To further understand the coupling between NCs and nanorods, we study the polarization properties of the PL spectra. Figure 4a−d show the dark-field scattering (a and b) and PL images (c and d) of NCs−Au nanorod composites collected from exactly the same locations at two polarization angles that are perpendicular to each other. For both scattering and PL, we find intensity differences of the spots in images with different analyzer angles. The polar plots of the scattering intensities of representative particles as a function of the analyzer angles are shown in Figure 4e. Since the strong dipolar LSPR of Au nanorods is inherently polarized along their major axis (longitudinal mode), the scattered light from the nanorod is also linearly polarized along the major axis.[42] Figure 4f shows the polar plots of PL intensities of the same nanosomposites. The PL from NCs attached to nanorods is also highly polarized along the major axis of the nanorod. We observed similar features for several spots in the images (see Supporting Information). The linearly polarized emission from randomly oriented emitters coupled to metal nanostructures was reported for Au nanorods coated with dye-doped silica shells[43] and Si NCs coupled to elongated silver nanoparticles.[15] We notice that the polarization of the emission from a single semiconductor NC, which in general depends on its shape, is almost isotropic for a spherical NC.[44,45] TEM images in Figure 1a and b clearly show the spherical shapes of our Si NCs. However, even in the presence of nonspherical NCs, the emission from an "ensemble" of NCs excited by unpolarized light is expected to be unpolarized due to the random orientation of the NCs.[46] In Figure 4g, we confirm this picture by comparing the polarized emission of Si NCs coupled and uncoupled to Au nanorods. The polarized emission from nanocomposites reflects the fact that the PL enhancement of Si NCs due to the plasmon coupling with longitudinal modes of Au nanorods is significantly larger compared to the excitation of the transverse modes. This results in a far-field emission that is polarized identically to the scattering of the longitudinal modes of Au nanorods. We will further confirm this interpretation in the next section based on our rigorous electromagnetic modeling results.

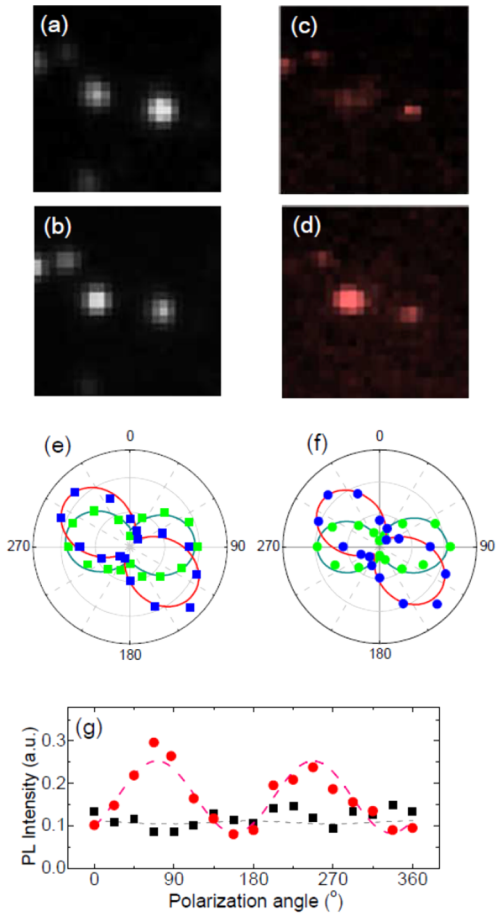

Figure 4. (a, b) Dark-field scattering and (c, d) PL images of NCs−Au nanorod composites at exactly the same region with different analyzer angles. The analyzer angles are perpendicular to each other. Polar plots of (e) scattering and (f) PL intensity of representative NCs−Au nanorod composites. Blue and green plots are obtained from identical nanocomposites, respectively. (h) PL intensities of nanocomposites (red) and ensemble Si NCs without Au nanorods (black) as a function of polarization angles.

DOI: 10.1021/acsphotonics.5b00233
ACS Photonics 2015, 2, 1298−1305

The enhancement of spontaneous emission rate in Figure 3 is explained by the enhancement of LDOS due to the LSPR of Au nanorods. To discuss the contribution of the radiative and nonradiative rates as well as the quantum efficiency of Si NCs-decorated Au nanorods, we performed theoretical calculations using the MNPBEM code,[33] which is based on the rigorous boundary element method. The decay rates in the vicinity of a Au nanorod with a diameter of 60 nm and a length of 126 nm have been simulated by placing point dipoles at fixed distances from the nanorod surface with tabulated dispersion data.[47] The results are normalized by the emission rate of a dipole in water, and thus we use the term radiative and nonradiative rate enhancements to describe the modification of decay rate due to the presence of a Au nanorod. In Figure 5a, we demonstrate a good agreement between the extinction spectra for Au nanorods obtained from experiment and the simulation. Figure 5b shows both radiative and nonradiative rate enhancements of a single dipole placed 10 nm from the top and side of a Au nanorod as a function of wavelength. The results are averaged over all dipole orientations. The largest enhancement of radiative rate is observed when the dipole is placed at the top of the nanorods. In contrast, when the dipole is positioned along the side of the nanorods, its radiative rate is small and comparable to the nonradiative rate at 750 nm. It is also worth noting that the radiative and nonradiative rate enhancement values, which determine the overall quantum efficiency of the plasmonic-coupled system,[48,49] strongly depend on the orientation of the dipoles. To discuss the quantum efficiency of the dipoles with different orientations, we compare the ratio of radiative to total decay rate enhancement, called the antenna efficiency.[48,49] In Figure 5c, we plot the results of a dipole oriented parallel (solid) and perpendicular (dashed) to the major axis of the nanorods. For dipoles placed at the side of the nanorod (black curves), the efficiency is comparable for both orientations. On the other hand, we find a dramatic change in the efficiency when a dipole at the top is oriented parallel to the major axis of the nanorod. This explains our experimental results of emission polarization in Figure 4f. In the case of NCs attached at the top of the nanorod, the PL intensity becomes much larger when the analyzer is positioned parallel to the major axis of the nanorods. The polarization-selective PL enhancement may improve the sensitivity and performance of bioimaging.

In our samples, NCs are randomly located on the surface of the Au nanorod. Therefore, we also took into account the relative effect of dipole positions around the nanorod and obtained the positionally averaged decay rates shown in Figure 5c. We notice that around the emission peak of NCs-750, the radiative rate enhancement is about 2 times larger than the nonradiative rate enhancement. Therefore, in nanocomposite of NC−Au nanorods, a significant quantum efficiency enhancement of the NCs can be obtained. The nonradiative decay becomes dominant at wavelengths shorter than 650 nm, which corresponds to the excitation region of the transverse scattering mode of the nanorods.

In order to quantitatively determine the quantum efficiency enhancement, we will now combine the experimental and theoretical results. We focus on the NCs-750 sample because the PL spectrum of NCs-750 fully overlaps with the LSPR of Au nanorods. The intrinsic quantum efficiency (Q_0) of Si NCs is expressed as $Q_0 = \gamma_r^0/(\gamma_r^0 + \gamma_{nr}^0)$, where γ_r^0 and γ_{nr}^0 are the intrinsic radiative and nonradiative decay rates of NCs in aqueous solution. The quantum efficiency of NCs coupled to Au nanorods (Q_m) is defined by

$$Q_m = \frac{\Gamma_r}{\Gamma_r + \Gamma_{abs} + \gamma_{nr}^0} \quad (1)$$

Here, Γ_r is the modified radiative rate, Γ_r/γ_r^0 corresponds to the Purcell factor[50−52] with respect to the emission of a dipole in water, and Γ_{abs} is the plasmon-induced nonradiative rate due to the absorption by the metallic nanorods. In eq 1, we assume that only the radiative rate is modified by the coupling with Au nanorods because the intrinsic nonradiative rate (γ_{nr}^0) arising from material imperfections of Si NCs is not affected by the local electromagnetic environment.[53,54] In fact, the decay rate

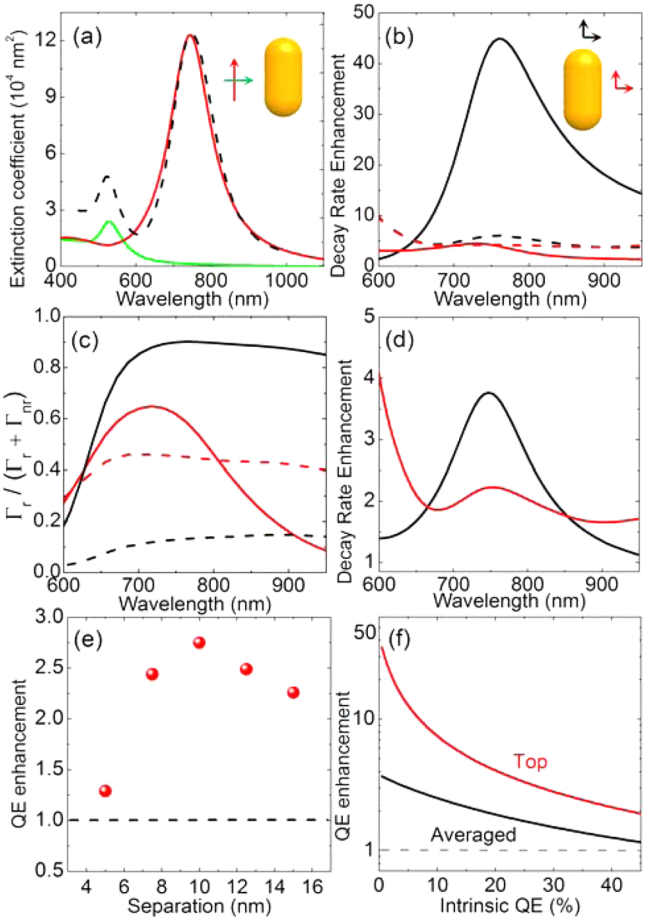

Figure 5. (a) Calculated extinction coefficient (solid line) of a Au nanorod excited by plane waves with two different polarizations (red and green curves) and measured extinction spectrum (dashed line). (b) Calculated radiative (solid line) and nonradiative (dashed line) decay rate enhancements of a dipole placed 10 nm from the top (black) and side (red) of a Au nanorod. The results are normalized by the radiative rate of the dipole in water and orientationally averaged. (c) Ratio between radiative and total decay rate enhancement of dipoles oriented parallel (solid) and perpendicular (dashed) to the long axis of the nanorods. Black and red curves represent the results of dipoles placed 10 nm from the top and side of the nanorods, respectively. (d) Both position- and orientation-averaged radiative (black) and nonradiative (red) decay rate enhancements. (e) Quantum efficiency enhancement as a function of separation between emitters and nanorods. (f) Quantum efficiency enhancements as a function of intrinsic quantum efficiency. Black and red curves represent positon-averaged results and the case of a dipole placed at the top of the nanorod, respectively.

DOI: 10.1021/acsphotonics.5b00233
ACS Photonics 2015, 2, 1298−1305

enhancement of NCs-750 shown in Figure 3e is almost unity at wavelengths that are detuned from the resonance of Au nanorods. This confirms that the measured decay rate enhancement is due to Γ_r/γ_r^0 (Purcell enhancement) and Γ_{abs}/γ_r^0 (absorption by Au nanorods) rather than modification of the internal nonradiative rate of Si NCs by coupling with nanorods.

By combining the experimentally obtained total decay rate enhancement (W_{total}) shown in Figure 3e with the Γ_r/γ_r^0 and Γ_{abs}/γ_r^0 values obtained from the simulations in Figure 5c, we can calculate Q_0, Q_m, and the enhancement of the quantum efficiency of Si NCs (see Supporting Information for calculation details). In Table 1, we summarize the results of

Table 1. Parameters of Emission of Si NCs at 750 nm: Measured Total Decay Rate Enhancement (W_{exp}), Radiative (Γ_r/γ_r^0) and Nonradiative (Γ_{abs}/γ_r^0) Decay Rate Enhancements from Simulation, Calculated Intrinsic (Q_0) and Modified (Q_m) Quantum Effciencies, and Calculated Quantum Efficiency Enhancement

λ (nm)	W_{exp}	Γ_r/γ_r^0	Γ_{abs}/γ_r^0	Q_0 (%)	Q_m (%)	quantum efficiency enhancement
750	1.35	3.77	2.23	7.4	20.7	2.8

emission at 750 nm, which is the NC emission peak. By coupling with Au nanorods, we found that the quantum efficiency of NC emission is enhanced by a factor of 2.8. We notice that this large enhancement is achieved only by engineering the radiative decay rate without the contribution from excitation enhancement (pumping enhancement). We also observe that the calculated Q_0 is in excellent agreement with the measured PL quantum yield (6.9 ± 0.7%) of our Si NCs in water,[30] which proves the validity of our analysis.

Finally, we discuss the perspective of the NC−Au nanorod composite. In this system, there are two determining factors for radiative rate enhancement, which are the NC location on the nanorod and their separation distance from the nanorod. In Figure 5e, we plot the quantum efficiency enhancement that can be obtained considering the emission of NCs with Q_0 = 7.4% (at 750 nm) as a function of their separation from the surface of a nanorod. The NC orientation and location around the surface of the nanorod have been averaged. We found that there exists an optimal separation distance in the range of 7.5 to 12.5 nm, which is very similar to the conditions of our samples. Figure 5f shows the quantum efficiency enhancement factors as a function of the intrinsic quantum efficiency of NCs. We plot both dipole position-averaged values as well as the case of a single dipole located at the top of the nanorod. From the curves of the position-averaged result, we demonstrate quantum efficiency enhancement in a wide range of values for the intrinsic quantum efficiency. This means that even in the case of emitters with significantly larger values of intrinsic quantum efficiency, the proposed plasmonic-coupled composites give rise to emission enhancement, especially when the emitters are located atop the nanorods. The selective binding of active molecules on top of nanorods has been already reported.[55−57] Although this work has been limited to Si NCs with low intrinsic quantum efficiency, the results of our numerical analysis demonstrate the applicability of the nanorod composite approach to other emitting materials that feature larger values of intrinsic quantum efficiency.

CONCLUSIONS

We have developed a novel plasmon-coupled light-emitting platform based on Au nanorods decorated by Si NCs. Through time-resolved PL measurements performed over a wide range of wavelengths, we have shown enhanced decay rates that follow the LSPR scattering spectrum of nanorods and tunable coupling efficiency of Si NCs with colloidal Au nanorods. The PL imaging and scattering maps of single nanocomposites demonstrate that the emission of Si NCs is polarized and driven by the efficient excitation of the longitudinal mode of Au nanorods. From a systematic PL analysis performed in partnership with rigorous theoretical calculations, we demonstrate a quantum efficiency enhancement of Si NCs up to approximately a factor of 3. To the best of our knowledge, this is the first experimental demonstration of plasmon-coupled nanocomposites based on Si NCs in an aqueous solution. Si-based plasmon-coupled nanocomposites prepared by a facile and cost-effective method are very promising candidates for the development of biocompatible fluorescent nanoprobes of interest to biosensing and bioimaging technologies.

ASSOCIATED CONTENT

Supporting Information

The Supporting Information is available free of charge on the ACS Publications website at DOI: 10.1021/acsphotonics.5b00233.

Additional TEM images, optical measurements, and calculations (PDF)

AUTHOR INFORMATION

Corresponding Author

*E-mail: dalnegro@bu.edu.

Notes

The authors declare no competing financial interest.

ACKNOWLEDGMENTS

This work was supported by KAKENHI through grants 23310077 and 24651143 (synthesis of silicon quantum dots), the U.S. Department of Energy, Office of Basic Energy Sciences, Division of Materials Science and Engineering, under Award DOE DE-SC0010679 to B.M.R. (nanorod−quantum dot hybrid material assembly), and partly (theoretical modeling) by the U.S. Army Research Laboratory through the Collaborative Research Alliance (CRA) for Multi Scale Multidisciplinary Modeling of Electronic Materials (MSME).

REFERENCES

(1) Pompa, P. P.; Martiradonna, L.; Torre, A. D.; Sala, F. D.; Manna, L.; De Vittorio, M.; Calabi, F.; Cingolani, R.; Rinaldi, R. Metal-Enhanced Fluorescence of Colloidal Nanocrystals with Nanoscale Control. *Nat. Nanotechnol.* **2006**, *1*, 126−130.

(2) Kinkhabwala, A.; Yu, Z.; Fan, S.; Avlasevich, Y.; Müllen, K.; Moerner, W. E. Large Single-Molecule Fluorescence Enhancements Produced by a Bowtie Nanoantenna. *Nat. Photonics* **2009**, *3*, 654−657.

(3) Jin, Y.; Gao, X. Plasmonic Fluorescent Quantum Dots. *Nat. Nanotechnol.* **2009**, *4*, 571−576.

(4) Ayala-Orozco, C.; Liu, J. G.; Knight, M. W.; Wang, Y.; Day, J. K.; Nordlander, P.; Halas, N. J. Fluorescence Enhancement of Molecules inside a Gold Nanomatryoshka. *Nano Lett.* **2014**, *14*, 2926−2933.

(5) Yao, J.; Yang, M.; Duan, Y. Chemistry, Biology, and Medicine of Fluorescent Nanomaterials and Related Systems: New Insights into Biosensing, Bioimaging, Genomics, Diagnostics, and Therapy. *Chem. Rev.* **2014**, *114*, 6130−6178.

DOI: 10.1021/acsphotonics.5b00233
ACS Photonics 2015, 2, 1298−1305

(6) Michalet, X.; Pinaud, F. F.; Bentolila, L. A.; Tsay, J. M.; Doose, S.; Li, J. J.; Sundaresan, G.; Wu, A. M.; Gambhir, S. S.; Weiss, S. Quantum Dots for Live Cells, in Vivo Imaging, and Diagnostics. *Science* **2005**, *307*, 538−544.
(7) Gao, X.; Cui, Y.; Levenson, R. M.; Chung, L. W. K.; Nie, S. In Vivo Cancer Targeting and Imaging with Semiconductor Quantum Dots. *Nat. Biotechnol.* **2004**, *22*, 969−976.
(8) Cohen-Hoshen, E.; Bryant, G. W.; Pinkas, I.; Sperling, J.; Bar-Joseph, I. Exciton-Plasmon Interactions in Quantum Dot-Gold Nanoparticle Structures. *Nano Lett.* **2012**, *12*, 4260−4264.
(9) Nepal, D.; Drummy, L. F.; Biswas, S.; Park, K.; Vaia, R. a. Large Scale Solution Assembly of Quantum Dot-Gold Nanorod Architectures with Plasmon Enhanced Fluorescence. *ACS Nano* **2013**, *7*, 9064−9074.
(10) Focsan, M.; Gabudean, A. M.; Vulpoi, A.; Astilean, S. Controlling the Luminescence of Carboxyl-Functionalized CdSe/ZnS Core−Shell Quantum Dots in Solution by Binding with Gold Nanorods. *J. Phys. Chem. C* **2014**, *118*, 25190−25199.
(11) Derfus, a M.; Chan, W. C. W.; Bhatia, S. N. Probing the Cytotoxicity of Semiconductor Quantum Dots, Supp. Info. *Nano Lett.* **2004**, *4*, 11−18.
(12) Resch-Genger, U.; Grabolle, M.; Cavaliere-Jaricot, S.; Nitschke, R.; Nann, T. Quantum Dots versus Organic Dyes as Fluorescent Labels. *Nat. Methods* **2008**, *5*, 763−775.
(13) Biteen, J. S.; Pacifici, D.; Lewis, N. S.; Atwater, H. a. Enhanced Radiative Emission Rate and Quantum Efficiency in Coupled Silicon Nanocrystal-Nanostructured Gold Emitters. *Nano Lett.* **2005**, *5*, 1768−1773.
(14) Takeda, E.; Fujii, M.; Nakamura, T.; Mochizuki, Y.; Hayashi, S. Enhancement of Photoluminescence from Excitons in Silicon Nanocrystals via Coupling to Surface Plasmon Polaritons. *J. Appl. Phys.* **2007**, *102*.02350610.1063/1.2753571
(15) Mertens, H.; Biteen, J. S.; Atwater, H. A.; Polman, A. Polarization-Selective Plasmon-Enhanced Silicon Quantum-Dot Luminescence. *Nano Lett.* **2006**, *6*, 2622.
(16) Walters, R. J.; Van Loon, R. V. a; Brunets, I.; Schmitz, J.; Polman, A. A. Silicon-Based Electrical Source for Surface Plasmon Polaritons. *IEEE Int. Conf. Gr. IV Photonics GFP* **2009**, *9*, 74−76.
(17) Goffard, J.; Gérard, D.; Miska, P.; Baudrion, A.-L.; Deturche, R.; Plain, J. Plasmonic Engineering of Spontaneous Emission from Silicon Nanocrystals. *Sci. Rep.* **2013**, *3*, 2672.
(18) Erogbogbo, F.; Yong, K.; Roy, I.; Xu, G.; Prasad, P. N.; Swihart, M. T. Biocompatible Luminescent Silicon. *ACS Nano* **2008**, *2*, 873−878.
(19) Mangolini, L.; Kortshagen, U. Plasma-Assisted Synthesis of Silicon Nanocrystal Inks. *Adv. Mater.* **2007**, *19*, 2513−2519.
(20) Pi, X.; Zhang, L.; Yang, D. Enhancing the Efficiency of Multicrystalline Silicon Solar Cells by the Inkjet Printing of Silicon-Quantum-Dot Ink. *J. Phys. Chem. C* **2012**, *116*, 21240−21243.
(21) Pi, X.; Yu, T.; Yang, D. Water-Dispersible Silicon-Quantum-Dot-Containing Micelles Self-Assembled from an Amphiphilic Polymer. *Part. Part. Syst. Charact.* **2014**, *31*, 751−756.
(22) Clark, R. J.; Dang, M. K. M.; Veinot, J. G. C. Exploration of Organic Acid Chain Length on Water-Soluble Silicon Quantum Dot Surfaces. *Langmuir* **2010**, *26*, 15657−15664.
(23) Sugimoto, H.; Fujii, M.; Imakita, K.; Hayashi, S.; Akamatsu, K. All-Inorganic Near-Infrared Luminescent Colloidal Silicon Nanocrystals: High Dispersibility in Polar Liquid by Phosphorus and Boron Codoping. *J. Phys. Chem. C* **2012**, *116*, 17969−17974.
(24) Sugimoto, H.; Fujii, M.; Imakita, K.; Hayashi, S.; Akamatsu, K. Codoping N- and P-Type Impurities in Colloidal Silicon Nanocrystals: Controlling Luminescence Energy from below Bulk Band Gap to Visible Range. *J. Phys. Chem. C* **2013**, *117*, 11850−11857.
(25) Fujii, M.; Toshikiyo, K.; Takase, Y.; Yamaguchi, Y.; Hayashi, S. Below Bulk-Band-Gap Photoluminescence at Room Temperature from Heavily P- and B-Doped Si Nanocrystals. *J. Appl. Phys.* **2003**, *94*, 1990−1995.
(26) Iori, F.; Degoli, E.; Magri, R.; Marri, I.; Cantele, G.; Ninno, D.; Trani, F.; Pulci, O.; Ossicini, S. Engineering Silicon Nanocrystals: Theoretical Study of the Effect of Codoping with Boron and Phosphorus. *Phys. Rev. B: Condens. Matter Mater. Phys.* **2007**, *76*, 1−14.
(27) Vinciguerra, V.; Franzò, G.; Priolo, F.; Iacona, F.; Spinella, C. Quantum Confinement and Recombination Dynamics in Silicon Nanocrystals Embedded in Si/SiO[sub 2] Superlattices. *J. Appl. Phys.* **2000**, *87*, 8165.
(28) Mastronardi, M. L.; Maier-Flaig, F.; Faulkner, D.; Henderson, E. J.; Kübel, C.; Lemmer, U.; Ozin, G. a. Size-Dependent Absolute Quantum Yields for Size-Separated Colloidally-Stable Silicon Nanocrystals. *Nano Lett.* **2012**, *12*, 337−342.
(29) Miller, J. B.; Van Sickle, A. R.; Anthony, R. J.; Kroll, D. M.; Kortshagen, U. R.; Hobbie, E. K. Ensemble Brightening and Enhanced Quantum Yield in Size-Purified Silicon Nanocrystals. *ACS Nano* **2012**, *6*, 7389−7396.
(30) Sugimoto, H.; Fujii, M.; Fukuda, Y.; Imakita, K.; Akamatsu, K. All-Inorganic Water-Dispersible Silicon Quantum Dots: Highly Efficient near-Infrared Luminescence in a Wide pH Range. *Nanoscale* **2014**, *6*, 122−126.
(31) Munechika, K.; Chen, Y.; Tillack, A. F.; Kulkarni, A. P.; Plante, I. J. La; Munro, A. M.; Ginger, D. S. Spectral Control of Plasmonic Emission Enhancement from Quantum Dots near Single Silver Nanoprisms. *Nano Lett.* **2010**, *10*, 2598−2603.
(32) Giannini, V.; Fernández-Domínguez, A. I.; Heck, S. C.; Maier, S. a. Plasmonic Nanoantennas: Fundamentals and Their Use in Controlling the Radiative Properties of Nanoemitters. *Chem. Rev.* **2011**, *111*, 3888−3912.
(33) Hohenester, U.; Trügler, A. MNPBEM - A Matlab Toolbox for the Simulation of Plasmonic Nanoparticles. *Comput. Phys. Commun.* **2012**, *183*, 370−381.
(34) Sugimoto, H.; Fujii, M.; Imakita, K.; Hayashi, S.; Akamatsu, K. Phosphorus and Boron Codoped Colloidal Silicon Nanocrystals with Inorganic Atomic Ligands. *J. Phys. Chem. C* **2013**, *117*, 6807−6813.
(35) Fujii, M.; Sugimoto, H.; Hasegawa, M.; Imakita, K. Silicon Nanocrystals with High Boron and Phosphorus Concentration Hydrophilic shell—Raman Scattering and X-Ray Photoelectron Spectroscopic Studies. *J. Appl. Phys.* **2014**, *115*, 084301.
(36) Rejman, J.; Oberle, V.; Zuhorn, I. S.; Hoekstra, D. Size-Dependent Internalization of Particles via the Pathways of Clathrin- and Caveolae-Mediated Endocytosis. *Biochem. J.* **2004**, *377*, 159−169.
(37) Focsan, M.; Gabudean, A. M.; Vulpoi, A.; Astilean, S. Controlling the Luminescence of Carboxyl-Functionalized CdSe/ZnS Core − Shell Quantum Dots in Solution by Binding with Gold Nanorods. *J. Phys. Chem. C* **2014**, *118*, 25190−25199.
(38) Lindsey, C. P.; Patterson, G. D. Detailed Comparison of the Williams−Watts and Cole−Davidson Functions. *J. Chem. Phys.* **1980**, *73*, 3348.
(39) Takeoka, S.; Fujii, M.; Hayashi, S. Size-Dependent Photoluminescence from Surface-Oxidized Si Nanocrystals in a Weak Confinement Regime. *Phys. Rev. B: Condens. Matter Mater. Phys.* **2000**, *62*, 16820−16825.
(40) Jin, S.; Demarco, E.; Pellin, M. J.; Farha, O. K.; Wiederrecht, G. P.; Hupp, J. T. Distance-Engineered Plasmon-Enhanced Light Harvesting in CdSe Quantum Dots. *J. Phys. Chem. Lett.* **2013**, *4*, 3527−3533.
(41) Abadeer, N. S.; Brennan, M. R.; Wilson, W. L.; Murphy, C. J. Distance and Plasmon Wavelength Dependent Fluorescence of Molecules Bound to Silica-Coated Gold Nanorods. *ACS Nano* **2014**, *8*, 8392−8406.
(42) Schubert, O.; Becker, J.; Carbone, L.; Khalavka, Y.; Provalska, T.; Zins, I.; Sönnichsen, C. Mapping the Polarization Pattern of Plasmon Modes Reveals Nanoparticle Symmetry. *Nano Lett.* **2008**, *8*, 2345−2350.
(43) Ming, T.; Zhao, L.; Chen, H.; Woo, K. C.; Wang, J.; Lin, H. Experimental Evidence of Plasmophores: Plasmon-Directed Polarized. *Nano Lett.* **2011**, *11*, 2296−2303.
(44) Peng, X.; Manna, L.; Yang, W.; Wickham, J.; Scher, E.; Kadavanich, A.; Alivisatos, A. Shape Control of CdSe Nanocrystals. *Nature* **2000**, *404*, 59−61.

DOI: 10.1021/acsphotonics.5b00233
ACS Photonics 2015, 2, 1298−1305

(45) Hu, J.; Li, L.-S.; Yang, W.; Manna, L.; Wang, L.-W.; Alivisatos, A. P. Linearly Polarized Emission from Colloidal Semiconductor Quantum Rods. *Science* **2001**, *292*, 2060−2063.
(46) Walters, R. J.; Kalkman, J.; Polman, A.; Atwater, H. A.; De Dood, M. J. A. Photoluminescence Quantum Efficiency of Dense Silicon Nanocrystal Ensembles in Si O2. *Phys. Rev. B: Condens. Matter Mater. Phys.* **2006**, *73*, 2−5.
(47) Johnson, P. B.; Christy, R. W. Optical Constants of the Noble Metals. *Phys. Rev. B* **1972**, *6*, 4370−4379.
(48) Novotny, L.; van Hulst, N. Antennas for Light. *Nat. Photonics* **2011**, *5*, 83−90.
(49) Busson, M. P.; Rolly, B.; Stout, B.; Bonod, N.; Bidault, S. Accelerated Single Photon Emission from Dye Molecule-Driven Nanoantennas Assembled on DNA. *Nat. Commun.* **2012**, *3*, 962.
(50) Purcell, E. M. Spontaneous Emission Probabilities at Radio Frquencies. *Phys. Rev.* **1946**, *69*, 674−674.
(51) Akselrod, G. M.; Argyropoulos, C.; Hoang, T. B.; Ciracì, C.; Fang, C.; Huang, J.; Smith, D. R.; Mikkelsen, M. H. Probing the Mechanisms of Large Purcell Enhancement in Plasmonic Nanoantennas. *Nat. Photonics* **2014**, *8*, 1−15.
(52) Lu, D.; Kan, J. J.; Fullerton, E. E.; Liu, Z. Enhancing Spontaneous Emission Rates of Molecules Using Nanopatterned Multilayer Hyperbolic Metamaterials. *Nat. Nanotechnol.* **2014**, *9*, 48−53.
(53) Govorov, A. O.; Bryant, G. W.; Zhang, W.; Skeini, T.; Lee, J.; Kotov, N. a; Slocik, J. M.; Naik, R. R. Exciton Plasmon Interaction and Hybrid Excitons in Semiconductor Metal Nanoparticle Assemblies. *Nano Lett.* **2006**, *6*, 984−994.
(54) Bharadwaj, P.; Novotny, L.; Bharadwaj, P.; Novotny, L. Spectral Dependence of Single Molecule Fluorescence Enhancement. *Opt. Express* **2007**, *15*, 14266.
(55) Caswell, K. K.; Wilson, J. N.; Bunz, U. H. F.; Murphy, C. J. Preferential End-to-End Assembly of Gold Nanorods by Biotin-Streptavidin Connectors. *J. Am. Chem. Soc.* **2003**, *125*, 13914−13915.
(56) Fu, Y.; Zhang, J.; Lakowicz, J. R. Plasmon-Enhanced Fluorescence from Single Fluorophores End-Linked to Gold Nanorods. *J. Am. Chem. Soc.* **2010**, *132*, 5540−5541.
(57) Chang, J.-Y.; Wu, H.; Chen, H.; Ling, Y.-C.; Tan, W. Oriented Assembly of Au Nanorods Using Biorecognition System. *Chem. Commun. (Cambridge, U. K.)* **2005**, 1092−1094.

DOI: 10.1021/acsphotonics.5b00233
ACS Photonics 2015, 2, 1298−1305